Journal of Medicinal Chemistry

Article

pubs.acs.org/jmc

Bcl-2/MDM2 Dual Inhibitors Based on Universal Pyramid-Like α-Helical Mimetics

Ziqian Wang,[†] Ting Song,[‡] Yingang Feng,[§] Zongwei Guo,[‡] Yudan Fan,[‡] Wenjie Xu,[†] Lu Liu,[†] Anhui Wang,[†] and Zhichao Zhang*[,†]

[†]State Key Laboratory of Fine Chemicals, School of Chemistry, Dalian University of Technology, No. 158-89, Zhongshan Road, Dalian 116012, People's Republic of China

[‡]School of Life Science and Technology, Dalian University of Technology, Dalian 116024, People's Republic of China

[§]Shandong Key Laboratory of Synthetic Biology, Qingdao Institute of Bioenergy and Bioprocess Technology, Chinese Academy of Sciences, Qingdao 266101, People's Republic of China

Supporting Information

ABSTRACT: No α-helical mimetic that exhibits Bcl-2/MDM2 dual inhibition has been rationally designed due to the different helicities of the α-helixes at their binding interfaces. Herein, we extracted a one-turn α-helix-mimicking *ortho*-triarene unit from *o*-phenylene foldamers. Linking benzamide substrates with a rotatable C−N bond, we constructed a novel semirigid pyramid-like scaffold that could support its two-turn α-helix mimicry without aromatic stacking interactions and could adopt the different dihedral angles of the key residues of p53 and BH3-only peptides. On the basis of this universal scaffold, a series of substituent groups were installed to capture the key residues of both p53TAD and BimBH3 and balance the differences of the bulks between them. Identified by FP, ITC, and NMR spectroscopy, a compound **6e** (**zq-1**) that directly binds to Mcl-1, Bcl-2, and MDM2 with balanced submicromolar affinities was obtained. Cell-based experiments demonstrated its antitumor ability through Bcl-2/MDM2 dual inhibition simultaneously.

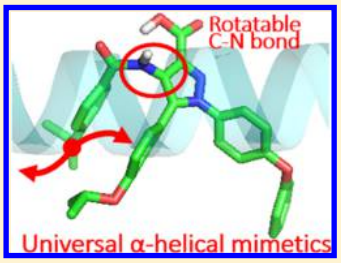

INTRODUCTION

The α-helical interfaces involved in protein−protein interactions (PPIs) are among the most attractive targets for medicinal chemistry because these PPIs play a key role in all cellular processes.[1] Artificial mimetics of α-helices that reproduce the arrangement of key side chains in an α-helix and match their topography and physicochemical properties have served as not only therapeutic agents but also research tools to understand PPIs.[2−5]

Of note, certain PPIs converge on the same cell signaling pathways and then exhibit cross-talk in the regulation of biological processes. For instance, the p53/MDM2 interaction and Bcl-2 family interactions are both central nodes in apoptosis.[6−9] Moreover, p53 has been recently identified as a new player in Bcl-2 family processes because the p53 released from MDM2 could directly interact with Bcl-2-like members.[10,11] Structural biological evidence further showed that Bcl-2 family proteins and MDM2 share a similar α-helical binding interface for p53TAD.[12−14] However, multitarget agents designed to target both p53/MDM2 and Bcl-2 interactions still remain to be discovered.

On the basis of the best-established nonpeptide terphenyl scaffold (represented by **1** in Scheme 1) that can mimic the i, i+3(i+4), and i+7 residues on a hydrophobic face of an α-helical peptide, a series of specific MDM2 inhibitors[15] and specific Bcl-2 inhibitors[16] whose affinities are in the submicromolar range were obtained. In addition to the lack of mimicking the hydrophilic residue i+5, the divergence in the i+3 key residues between the p53TAD and BH3-only proteins make it difficult for terphenyl analogues to adapt to the two targets simultaneously.[15,16]

Scheme 1. Structure of Compounds 1−4

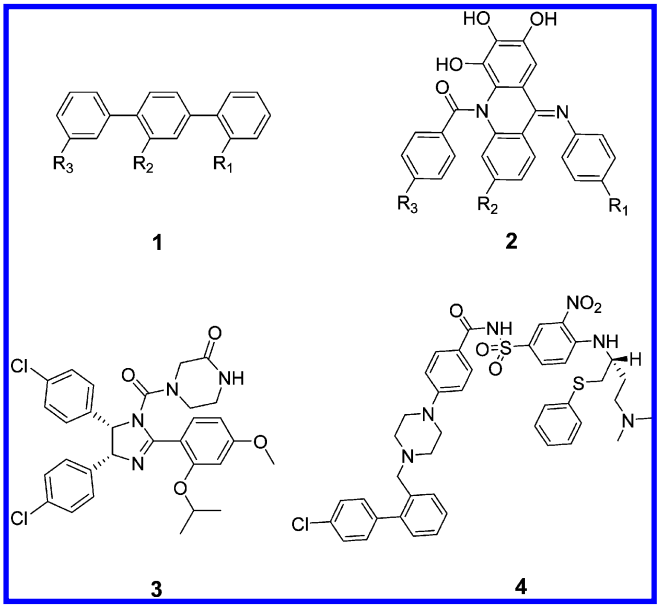

Received: December 11, 2015
Published: March 16, 2016

DOI: 10.1021/acs.jmedchem.5b01913
J. Med. Chem. 2016, 59, 3152−3162

The two-faced α-helix-mimicking cross-acridine scaffold[17] (**2** in Scheme 1) reported by our group could extensively mimic the i, i+3, i+5, and i+7 residues on both the hydrophobic and the hydrophilic faces of an α-helical peptide and showed affinities in approximately the 10 nM range toward Bcl-2 and Mcl-1. However, rotation of the aromatic amide and imine bonds of **2** are restricted, which led to the poor mimicking of the α-helixes of p53 and BH3-only peptide simultaneously, whose hot-spot residues exhibit different dihedral angles, as discussed in the following text. Thus, the cross-acridine compounds cannot fit MDM2 though they could be accommodated by the BH3 groove of Bcl-2/Mcl-1.

Foldamers,[18] defined as artificial folded molecular architectures, are considered to form regions of ordered helical structure. However, none of the traditional foldamers has been applied as an α-helix mimetic due to a mismatch of their diameters with α-helixes.

The recently described *o*-phenylenes[19,20] represent a new class of helical polymers and foldamers, stabilized by aromatic stacking interactions. Although their diameter is similar to that of α-helixes, this scaffold cannot project hotspot-mimicking substituents to the proper apposition because substituent effects could disturb the aromatic stacking interactions.

So far, the only reported "Bcl-2/p53 dual inhibitor" is the known MDM2-specific inhibitor **3** (Nutlin-3a, Scheme 1),[21] which was recently found by NMR to bind to Bcl-2.[10,14,22] However, its much lower affinity to Bcl-2 (15 μM) than to MDM2 (35 nM) failed to translate into the induction of Bcl-2-targeted apoptosis in cell-based examinations, as described in this study.

As such, there is neither a universal scaffold to adopt the α-helix of both MDM2 and BH3-only peptide nor a Bcl-2/MDM2 dual inhibitor.

In this study, we constructed a novel semirigid pyramid-like scaffold that could adopt the α-helix of both MDM2 and BH3-only peptides. On the basis of this universal scaffold, a compound, **6e**, which directly binds to Mcl-1, Bcl-2, and MDM2, was obtained. Its balanced submicromolar affinities toward three targeted proteins translated into the effective disruption of Bcl-2/Bax, Mcl-1/Bak, and p53/MDM2 in cancer cells and showed advantages over compounds **3** and **4** (ABT-737, Scheme 1),[23] as it induced cell cycle arrest in addition to apoptosis through Bcl-2/MDM2 simultaneous inhibition. This first Bcl-2/MDM2 dual inhibitor may not only serve as a synergistic antitumor therapy but could also be applied to investigate the cross-talk between the two apoptotic pathways.

RESULTS AND DISCUSSION

Rational Design and Synthesis of a Universal α-Helix-Mimicking Scaffold. We first compared the crystallographic results of the p53/MDM2 (PDB 1YCR),[24] Bim/Mcl-1 (PDB 2PQK),[25] and Bim/Bcl-xl (PDB 1PQ1)[26] complexes (Figure 1a,b). They feature α-helical segments in their interfaces though p53TAD is not completely in the α-helical conformation over the stretch covering the three key residues. Three key residues sharing the same hydrophobic character and positions at i, i+3 (i+4), and i+7 (L62, I65, and F69 in BimBH3, respectively, and F19, W23, and L26 in p53TAD, respectively) are distributed along the hydrophobic face of two-turns of α-helixes.[14,27] A hydrophilic key residue D67 at the position i+5 of BimBH3 peptide on the opposite side served as a key residue for both Bim/Mcl-1 and Bim/Bcl-2 interactions, while D21 (i+2) shares the same hydrophilic properties and position with D67 in p53TAD. The relative positions of these residues are shown in Figure 1a,b.

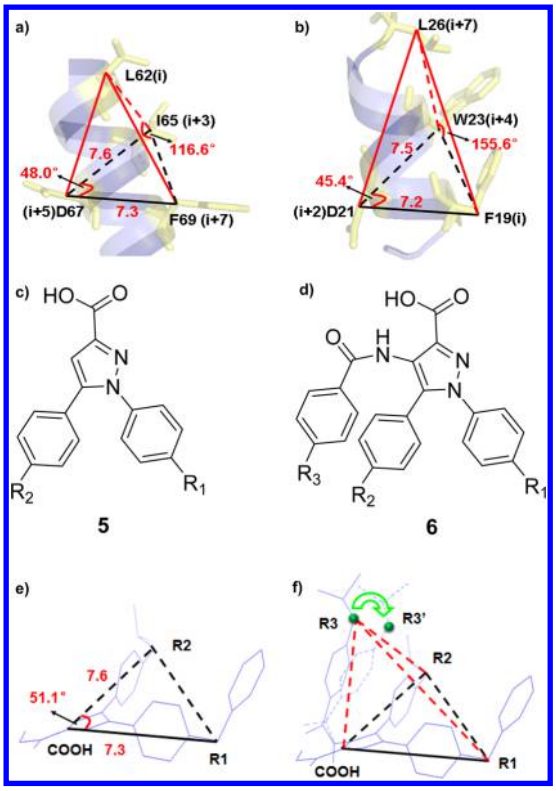

Figure 1. (a) Representation of an α-helix in Bim showing L62 (i), I65 (i+3), D67 (i+5), and F69 (i+7) residues. (b) Representation of an α-helix in p53 showing F19 (i), D21 (i+2), W23 (i+4), and L26 (i+7) residues. (c) Structure of *ortho*-triarene derivatives **5**. (d) Structure of *ortho*-triarene derivatives **6**. (e) Lowest-energy conformation of α-helix mimetic **5g**. (f) Lowest-energy conformation of α-helix mimetic **6e**.

Notably, when i+3 (i+4), i+5 (i+2), and i+7 (i) residues construct a triangle conformation like the bottom of a pyramid (indicated in black in Figure 1a,b) with similar side length and angle between BimBH3 and p53TAD. There is a significant discrepancy in the height of the pyramids which results from the difference in helicities of the two α-helixes. The angle between the i residue (L62 in BimBH3) and the pyramid bottom is 116.6°, while the corresponding angle between the i +7 residue (L26 in p53TAD) and the bottom is 155.6°.

As such, a scaffold that could both rigidly maintain a triangle bottom and exhibit some flexibility to adjust the height of the pyramid-like structure is considered as an imperative structural feature of a universal α-helical mimetic.

We then extracted an *ortho*-triarene unit from *o*-phenylene foldamers to mimic a one-turn α-helix (represented by **5** in Figure 1c), which could keep a rigidly triangle conformation with stable side length and angle without aromatic stacking interactions. With the hydrophobic R_1 and R_2 and the hydrophilic COOH groups, this template exhibited similar side length and angle with the triangle bottom of the pyramid-like model (Figure 1e). Then, a rotatable C−N single bond linked benzamide was introduced at the 4-position to extend to mimic a two-turn α-helix (scaffold **6** in Figure 1d). R_3 was attached to benzamide group to mimic the i (i+7) residue (L62 in Bim and L26 in p53) (Figure 1f). In this way, **6** serves as a pyramid-like scaffold, and the rotation of the C−N single bond could modulate the distance and angle between R_3 and the

DOI: 10.1021/acs.jmedchem.5b01913
J. Med. Chem. 2016, 59, 3152−3162

Scheme 2. Synthesis of Compounds 5a−5i[a]

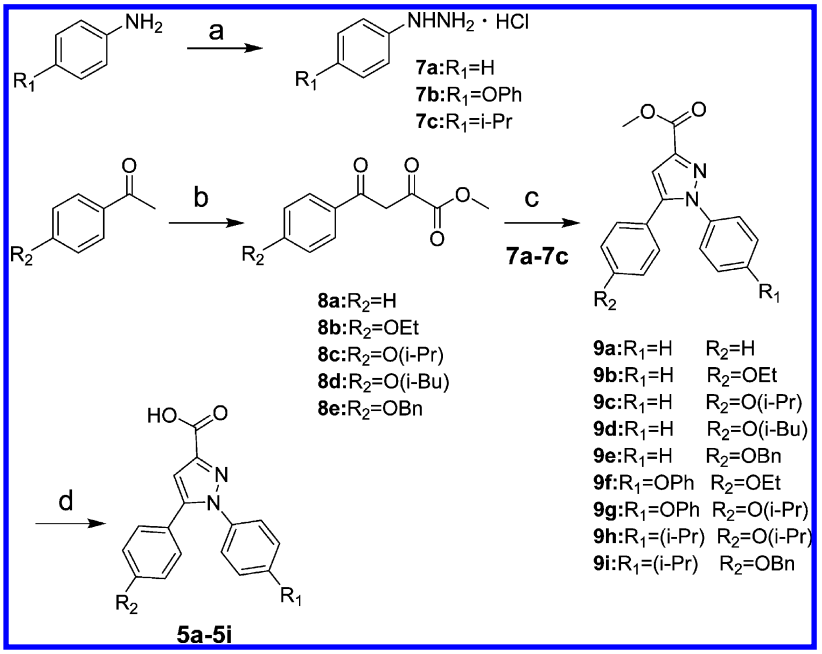

[a](a) $NaNO_2$, hydrochloric acid, $SnCl_2$, 0 °C,4 h; (b) dimethyl oxalate, potassium *tert*-butoxide, THF, 0 °C to room temp, 16 h, 76−87%; (c) phenylhydrazine hydrochloride **7a**−**7c**, MeOH, 65 °C, 3 h, 49−62%; (d) KOH, MeOH, 60 °C,4 h, 87−96%.

Scheme 3. Synthesis of Compounds 6a−6h[a]

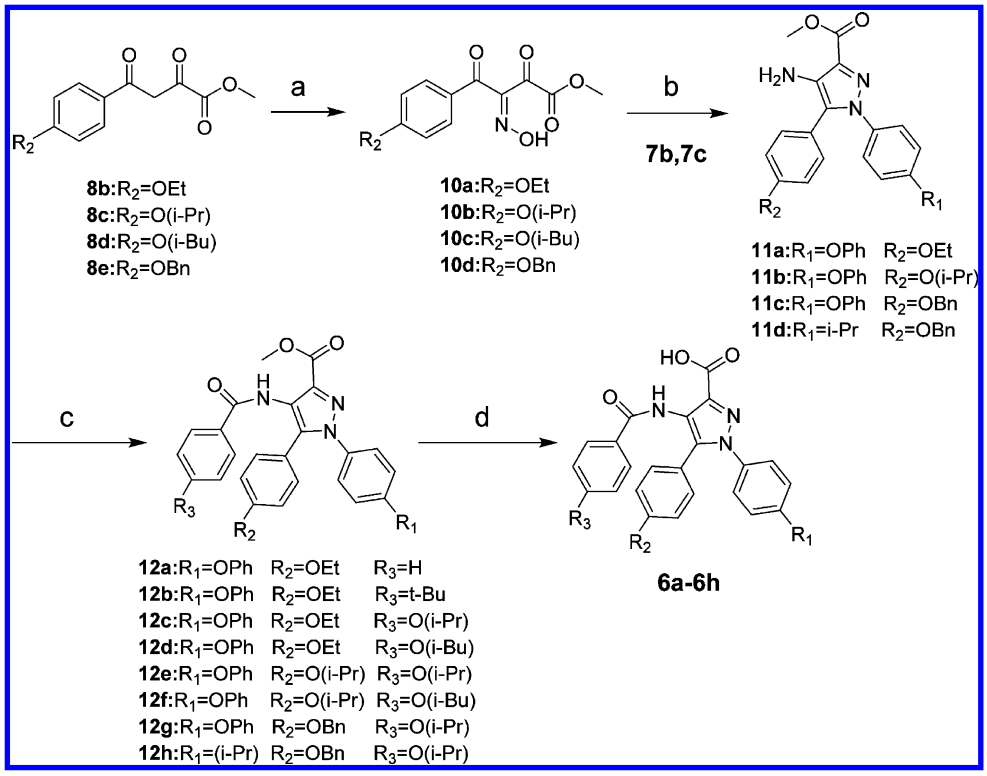

[a](a) N_2O_3, MeOH, room temp, 2 h; (b) phenylhydrazine hydrochloride **7b**, **7c**, MeOH, argon atmosphere, 6 h, $Na_2S_4O_6$, 21−25% over two steps; (c) 4-R_3-benzoyl chloride, triethylamine, THF, 0 °C, 76−86%; (d) NaOH, 0 °C, THF:H_2O = 2:1, 85−95%.

functional groups on the pyramid bottom, which makes it possible for its derivatives to adopt to α-helixes with different helicities.

A modular synthesis of scaffolds **5** and **6** are shown in Schemes2 and 3. Briefly, a para-substituted acetophenone was treated with dimethyl oxalate to obtain **8**. Then **9** was obtained by **8** and para-substituted phenylhydrazine **7**, prepared by commercially available anilines.[28] Moreover, treating **8** with N_2O_3 and then **9** in a one-pot step led to the methyl 4-amino-1,5-diphenyl-1*H*-pyrazole-3-carboxylate analogue **11**. Reaction

DOI: 10.1021/acs.jmedchem.5b01913
J. Med. Chem. 2016, 59, 3152−3162

Table 1. Structure and Binding Affinities of α-Helix Mimetics with Mcl-1, Bcl-2, and MDM2 Determined by FP

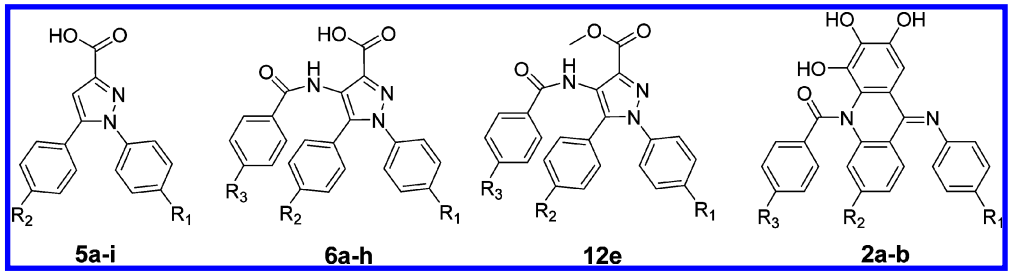

compd	R_1	R_2	R_3	K_i ± SD (Mcl-1) [μM]	K_i ± SD (Bcl-2) [μM]	K_i ± SD (MDM2) [μM]
5a	H	H		>10	>10	>25
5b	H	OEt		3.80 ± 0.95	6.09 ± 1.12	3.26 ± 0.88
5c	H	O(*I*-Pr)		3.62 ± 1.32	7.00 ± 2.54	2.29 ± 0.64
5d	H	O(*i*-Bu)		8.11 ± 1.63	>10	7.42 ± 2.81
5e	H	OBn		>10	>10	19.8 ± 3.5
5f	OPh	OEt		0.451 ± 0.164	0.694 ± 0.055	1.03 ± 0.441
5g	OPh	O(*i*-Pr)		0.371 ± 0.139	0.932 ± 0.218	0.712 ± 0.155
5h	*i*-Pr	O(*i*-Pr)		2.39 ± 0.86	5.25 ± 0.38	2.14 ± 0.91
5i	*i*-Pr	OBn		0.226 ± 0.032	0.385 ± 0.027	0.616 ± 0.060
6a	OPh	OEt	H	0.635 ± 0.033	0.855 ± 0.018	1.13 ± 0.49
6b	OPh	OEt	*t*-Bu	0.404 ± 0.064	0.406 ± 0.108	0.689 ± 0.037
6c	OPh	OEt	O(*i*-Pr)	0.081 ± 0.011	0.028 ± 0.008	0.301 ± 0.032
6d	OPh	OEt	O(*i*-Bu)	0.393 ± 0.030	1.04 ± 0.22	0.446 ± 0.056
6e	OPh	O(*i*-Pr)	O(i-Pr)	0.161 ± 0.039	0.140 ± 0.013	0.107 ± 0.018
6f	OPh	O(*i*-Pr)	O(*i*-Bu)	0.722 ± 0.045	1.40 ± 0.49	0.422 ± 0.102
6g	OPh	OBn	O(*i*-Pr)	>10	>10	4.47 ± 0.91
6h	*i*-Pr	OBn	O(*I*-Pr)	2.60 ± 0.44	>10	2.19 ± 0.34
12e	OPh	O(*i*-Pr)	O(*i*-Pr)	4.52 ± 0.30	5.16 ± 0.62	4.28 ± 1.05
2a	Me	Me	*t*-Bu	0.247 ± 0.135	0.207 ± 0.166	24.3 ± 4.6
2b	OPh	*i*-Pr	*t*-Bu	0.079 ± 0.022	0.056 ± 0.028	>25
(−)-gossypol				0.260 ± 0.034	0.431 ± 0.076	>25
3				>10	>10	0.059 ± 0.033

of **11** and para-substituted benzoyl chlorides afforded **12**. Compounds **9** and **12** could be further selectively hydrolyzed to the target compounds **5** and **6**.[29]

Structure−Activity Relationship of p53/Bcl-2 Dual Inhibitors. On the basis of scaffolds **5** and **6**, a library of analogues with different substrates was prepared through a modular synthesis. The specific binding effects of these molecules on targeted protein−protein complexes were evaluated through fluorescence polarization assays (FP). BimBH3 and p53TAD peptides were labeled with fluorescein as the probe to monitor the competitive binding of these compounds to Mcl-1/Bcl-2 and MDM2, respectively. The traditional Mcl-1/Bcl-2 inhibitor (−)-gossypol and MDM2 inhibitor **3** were used as controls (Table 1 and Supporting Information, Figure S1).

The R_2 group that mimics the I65 in Bim and W23 in p53 was first explored. We hypothesized that this site may correspond to the selectivity between MDM2 and Bcl-2 because according to the X-ray crystallographic data, the I65 and W23 residues project from the same position of the α-helix but show significant differences in steric bulk (Figure 1a,b). Our FP results showed that when the scaffold with only carboxyl (compound **5a** in Table 1) showed no binding with either Bcl-2-like or MDM2 protein, low micromolar affinities appeared for all the three proteins for compounds **5b** and **5c**, which bear a hydrophobic R_2 group. Compared with compound **5d** and **5e**, the OEt group of **5b** and the O(*i*-Pr) group of **5c** are appropriate groups to balance the difference between I65 in BimBH3 and W23 in p53TAD.

Next, we substituted OPh as the R_1 group to mimic F69 in Bim and F19 in p53, yielding compounds **5f** and **5g**. A significantly improved ability to bind to Mcl-1 and Bcl-2 (approximately 10-fold better binding compared to **5b** and **5c**), which was in the submicromolar range, was found, and a moderate improvement was found for MDM2 binding (3-fold). The *i*-Pr group of the compounds **5h** and **5i** did not increase the affinities for the three proteins due to the much smaller bulks which cannot occupy the corresponding binding pocket very well.

Strong support was also provided by molecular modeling studies (Figure 2a,b); these revealed that the three substituted positions (R_1, R_2, and COOH) of compound **5g** occupied the binding positions for the I65, D67, and F69 of BimBH3 (Figure 2a), while R_1 and R_2 occupied the binding positions for the W23 and F19 of p53TAD in a similar manner. As expected, the COOH of **5g** could not match the orientation of D21 in p53TAD and pointed directly into water when binding to MDM2 (Figure 2b).

So far, we have obtained compounds **5f** and **5g** as new scaffolds to stably mimic both hydrophilic and hydrophobic key residues on one α-helical turn featured by different PPIs. We then applied a rotatable C−N to link R_3 substituents to grab one more hydrophobic residue (L62 (i) in Bim and L26 (i+7) in p53) located on the adjacent turn of the α-helix, specifically,

DOI: 10.1021/acs.jmedchem.5b01913
J. Med. Chem. 2016, 59, 3152−3162

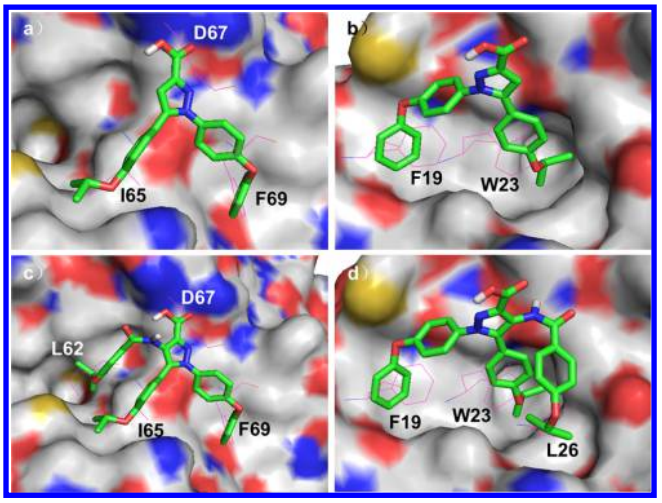

Figure 2. Predicted binding models of the *ortho*-triarene derivatives in complex with Mcl-1 and MDM2. (a) Docking of compound **5g** to Mcl-1. (b) Docking of compound **5g** to MDM2. (c) Docking of compound **6e** to Mcl-1. (d) Docking of compound **6e** to MDM2.

to fit the different helicities between p53TAD and BH3-only peptide.

R_3 groups with a progressive increase in steric bulk were attached, yielding compounds **6a**, **6b**, **6c**, and **6d**. An increase in affinities toward all the three targeted proteins was found and this affinity was maximized for compound **6c**, which bears an *iso*-propoxyl group as R_3. **6c** could competitively displace the BH3 peptide from all of these three proteins with a good potency (K_i = 0.081 μM to Mcl-1, 0.028 μM to Bcl-2, and 0.301 μM to MDM2). However, compound **6d**, with a larger O(*I*-Bu) R_3 group, did not greatly affect the affinity for MDM2 but led to an obvious decrease in the binding affinities to Mcl-1/Bcl-2 (approximately 5-fold), which is consistent with the fact that the hydrophobic pocket occupied by R_3 in MDM2 is bigger than that in Bcl-2 family members.[15,16] These results suggested that the O(*i*-Pr) group here achieved the best functional mimicry of both L62 in Bim and L26 in p53. Notably, when we enlarged the R_2 group to O(*i*-Pr) based on **6c**, the most balanced affinities in the submicromolar range toward all three proteins (0.161 μM to Mcl-1, 0.140 μM to Bcl-2, and 0.107 μM to MDM2) was found for compound **6e**. The further enlargement of the R_2 group or both R_2 and R_3 groups decreased the affinities of compounds **6f**, **6g**, and **6h**, suggesting the substituents of compound **6e** best compromised the difference between the hydrophobic key residues of BimBH3 and p53TAD.

A docking simulation of **6e** further supported that the binding grooves of BimBH3 and p53TAD on the surface of Mcl-1, Bcl-2, and MDM2 are the target areas for this synthetic proteomimetic (Figure 2c,d). The top-ranked binding modes were all positioned in the traditional binding clefts and covered the hydrophobic "hot-spots" occupied by the i, i+3 (i+4), and i +7 residues in the α-helixes in the BimBH3 and p53TAD domains. Similar to compound **5g** (Figure 2a,b), the COOH of compound **6e** occupied the position of D67 in BimBH3 when binding to Mcl-1 (Figure 2c), while the same COOH pointed directly into water when binding to MDM2 (Figure 2d).

Additionally, alanine scanning mutagenesis showed that D67 of the BimBH3 peptide served as a key residue for both Bim/Mcl-1 and Bim/Bcl-2 interactions,[25] while D21, which shares the same hydrophilic properties and position with D67, contributes little to p53/MDM2 interactions.[6] We thus attempted to probe the contribution of this hotspot to a universal small-molecular inhibitor. We converted R_3 to methyl ester, which resulted in a significant reduction in activity for compound **6e** binding to the three proteins. While the lost affinity toward Bcl-2 and Mcl-1 is not surprising because we previously identified D67 as the hottest spot for the two

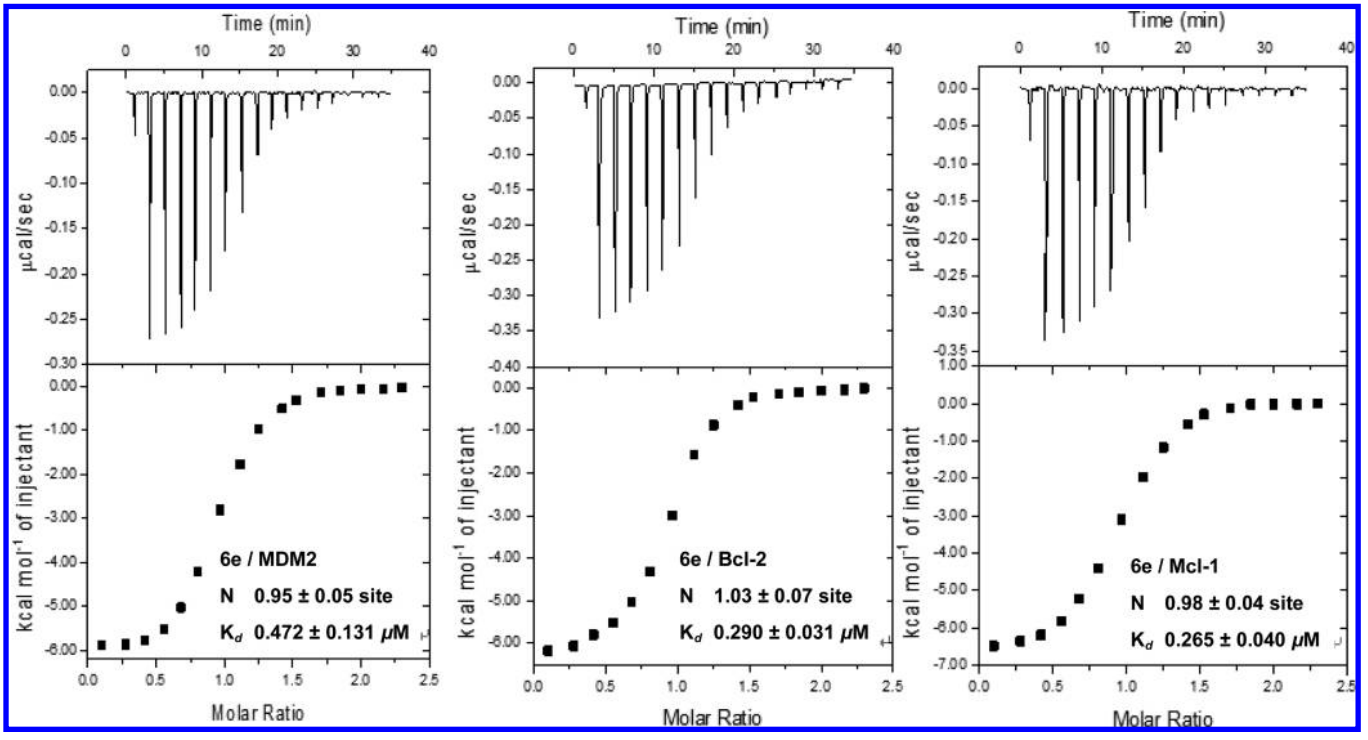

Figure 3. Heat effects of **6e**/MDM2, **6e**/Bcl-2, and **6e**/Mcl-1 dimer dissociations measured by ITC.

DOI: 10.1021/acs.jmedchem.5b01913
J. Med. Chem. 2016, 59, 3152−3162

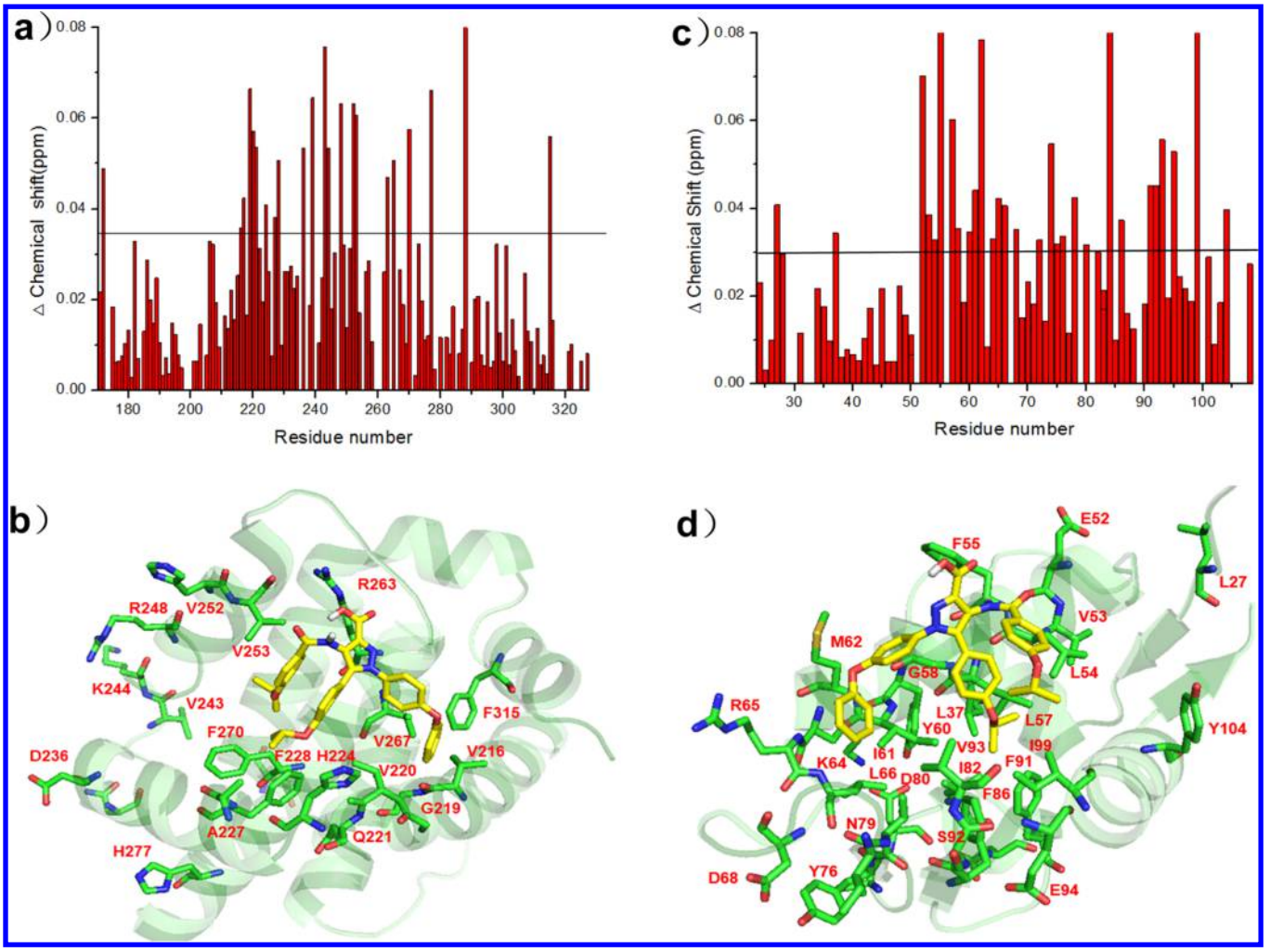

Figure 4. NMR characterization of the interaction between Mcl-1 and compound **6e**. The $^{15}N-^{1}H$ heteronuclear single quantum coherence (HSQC) NMR spectroscopy of ^{15}N-labeled Mcl-1 titrated with compound **6e** in a ratio of 1:1 was compared with that of ^{15}N-labeled Mcl-1 in free form. (a) Chemical shift perturbations of Mcl-1 residues when bound to **6e**. (b) NMR-derived structure of **6e** bound to Mcl-1. Mcl-1 residues with chemical shift changes >0.035 ppm are shown. (c) Chemical shift perturbations of MDM2 residues when bound to **6e**. (d) NMR-derived structure of **6e** bound to MDM2. MDM2 residues with chemical shift changes >0.030 ppm are shown.

proteins,[30] it is unexpected that compound **12e** also showed a much lower affinity to MDM2 (5-fold lower than **6e**). This suggested that the hydrophilic group could at least contribute to the positioning of the molecule within the pocket and help the hydrophobic substituents of the molecule to orient into the hydrophobic pocket, even if it cannot interact with the protein directly.

As expected, the cross-acridine mimetics earlier reported by our group, shown as compound **2a** and **2b** (Table 1), exhibited obvious selectivity between Bcl-2/Mcl-1 and MDM2. The planar structure feature of these molecules resulted from the hardly rotatable amido bond, and the large conjugated system may be responsible for this selectivity between these similar targets.

So far, **6e** was identified as a universal α-helical mimicry whose balanced submicromolar affinities toward Bcl-2, Mcl-1, and MDM2 may provide unique functions based on Bcl-2/p53 dual inhibition.

To further identify direct multitarget binding ability, ITC was performed on **6e** for Mcl-1, Bcl-2, and MDM2. As shown in Figure 3, **6e** exhibited balanced submicromolar range affinities for MDM2 (K_d = 0.472 μM), Bcl-2 (K_d = 0.290 μM), and Mcl-1 (K_d = 0.265 μM), which were consistent with the FP results.

Binding Mode Identification of 6e. Heteronuclear single quantum coherence (HSQC) NMR spectroscopy using ^{15}N-labeled Mcl-1 and MDM2 was performed to investigate the binding site of **6e** (Figure 4 and Supporting Information, Figure S2). More than 80% of the residues showing significant chemical shift changes (>0.035 ppm) upon addition of compound **6e** were located in the BimBH3 binding domain of Mcl-1 (Figure 4a). Residue R263 interacted with D67 and its neighboring residues R248, H252, V253, and V265 showed significant changes in chemical shift upon the addition of **6e**. V243, V252, V253, and F270, which construct the pocket to accommodate L62; Q221, H224, A227, F228, and V267 to form the pocket for I65; and V216, G217, G219, V220, and F319 for F69 were also significantly affected. Additionally, D236, K244, and H277, which do not contact **6e** directly, also showed significant chemical shift perturbations, probably as a result of changes in the chemical environment as the groove opened to accommodate **6e** (Figure 4b). Also, more than 80% of the residues showing significant chemical shift changes (>0.030 ppm) upon addition of compound **6e** were located in

DOI: 10.1021/acs.jmedchem.5b01913
J. Med. Chem. 2016, 59, 3152−3162

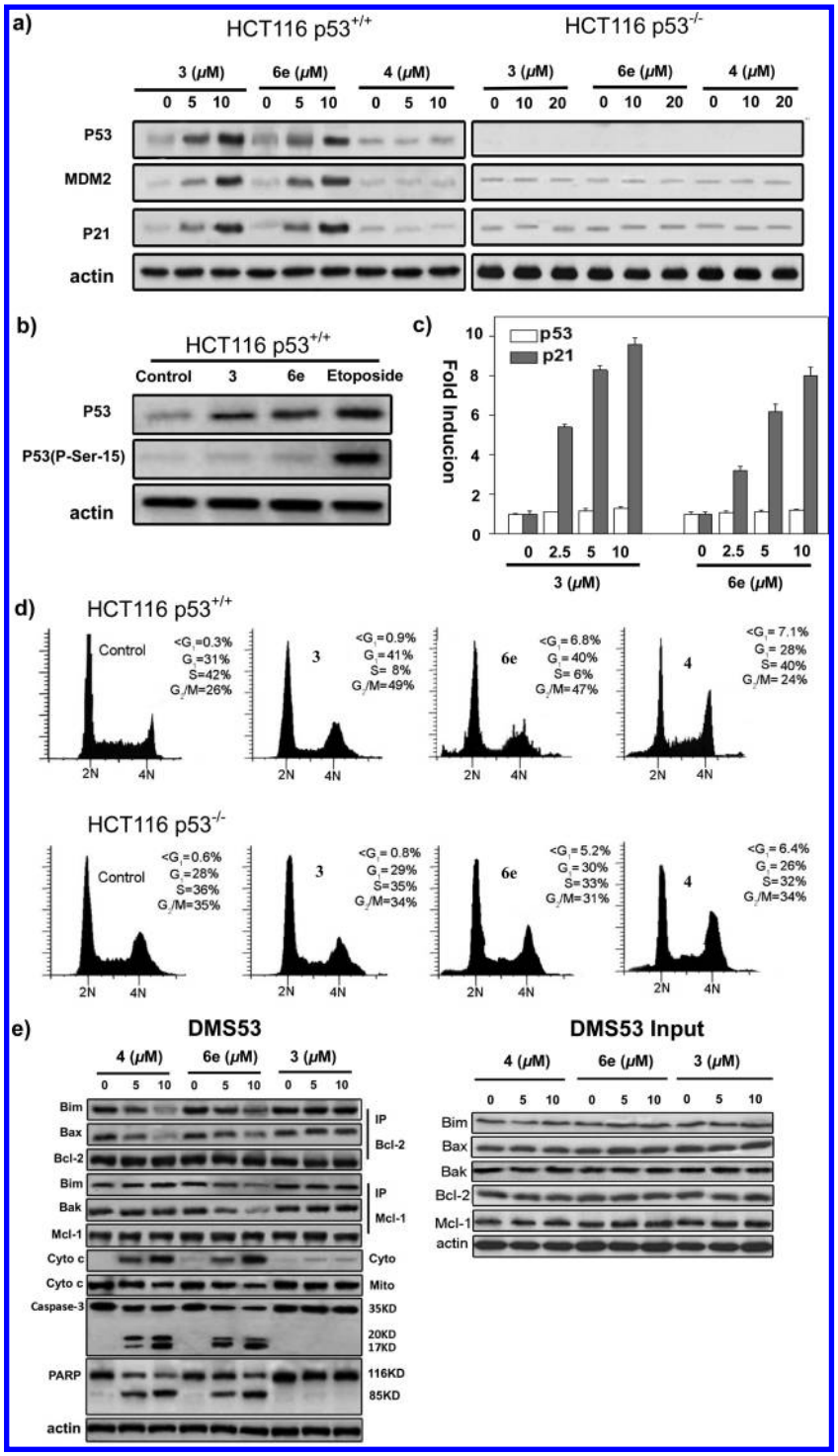

Figure 5. Targeting MDM2 and Bcl-2/Mcl-1 by **6e** activates the p53 pathway in cells with wild-type p53 and the intrinsic apoptosis pathway in cells with Bax/Bak. (a) HCT116 $p53^{+/+}$ and HCT116 $p53^{-/-}$ cells were incubated with the indicated concentrations of compounds **3**, **6e**, or **4** for 12 h and p53, p21, and MDM2 proteins were analyzed in the cell lysates by immunoblotting. (b) HCT116 $p53^{+/+}$ cells were treated with compound **3** (5 μM), **6e** (5 μM), or the genotoxic drug etoposide (10 μM, which causes phosphorylation of p53 at Ser^{15}) for 24 h, and the amounts of total p53 and p53 phosphorylated at Ser^{15} were analyzed in the cell lysates by immunoblotting. (c) HCT116 $p53^{+/+}$ cells were treated with the indicated concentrations of compounds **3** or **6e** for 12 h, and the change in the level of transcription was measured by quantitative PCR and expressed as fold induction compared with the untreated control. (d) HCT116 $p53^{+/+}$ cells were treated with compounds **3** (5 μM), **6e** (5 μM), or **4** (5 μM) for 24 h (the first line), and HCT116 $p53^{-/-}$ cells were treated with compounds **3** (10 μM), **6e** (10 μM), or **4** (10 μM) for 24 h (the second line). Cell cycle distribution was analyzed by PI staining. (e) Bcl-2 and Mcl-1, respectively, were immunoprecipitated from DMS53 cells treated with the indicated concentrations of **6e** or **4** for 12 h, and immunoprecipitates were subjected to immunoblotting analysis for Bim, Bax, and Bak proteins. In parallel, cytosolic release of cytochrome c and cleavage of caspase-3 and PARP were assessed by immunoblotting (left). The input represented 10% of the whole-cell lysate used for each immunoprecipitation (right).

DOI: 10.1021/acs.jmedchem.5b01913
J. Med. Chem. 2016, 59, 3152−3162

the p53TAD binding domain of MMD2 (Figure 4c). I61, M62, K64, and I66, which construct the pocket to accommodate F19; G58, I60, I82, F86, and V93 to form the pocket for W23; and V53, V54, F91, and I99 for I26 were also significantly affected. Additionally, L27, R65, and D68, which do not contact **6e** directly, also showed significant chemical shift perturbations, probably as a result of changes in the chemical environment as the groove opened to accommodate **6e** (Figure 4d). The NMR results demonstrate that **6e** accurately mimics the L62, I65, F69, and D67 residues of BimBH3 and the F19, W23, and I26 residues of p53TAD.

Because of the overall similar binding cleft and hotspot arrangements of Mcl-1 and Bcl-2, we believe **6e** binds to Bcl-2 in a manner similar to its binding to Mcl-1.

Antitumor Ability of 6e Based on Dual-Target Inhibition of Bcl-2 and MDM2. Next, we examined whether the in vitro dual inhibition of **6e** could translate into dual-targeted antitumor ability against tumor cells. Compound **6e** exhibited 5−7 μM IC_{50} values on both MDM2-dependent and Bcl-2-dependent cell lines (HCT116 $p53^{+/+}$ and DMS 53, Supporting Information, Table S1).

To examine MDM2 targeting in the cellular context, the effect of **6e** on the expression levels of p53, MDM2, and p21 was first tested in HCT116 $p53^{+/+}$ cells which express abundant wild-type p53 protein. Compounds **3** and **4** were tested in parallel as a negative and positive control, respectively. As shown in Figure 5a (left), **6e** treatment led to a dose-dependent increase in the levels of p53, MDM2, and p21 in cells, resembling the effects of **3**. The stabilization and accumulation of these three proteins are characteristic consequences of inhibition of MDM2-p53 binding. By contrast, compound **4** had no such effects. Consistent with on-target inhibition of MDM2 by **6e**, loss of MDM2-p53 target in HCT116 $p53^{-/-}$ cells abolished its effects on the three responsive proteins (Figure 5a, right). Second, we confirmed that **6e** activated p53 by targeting MDM2 rather than causing p53 phosphorylation or changing p53 mRNA level even at the highest concentration tested (10 μM), which has caused an 8-fold induction of p21 mRNA (Figure 5b,c), excluding a genotoxic or transcriptional mechanism to activate p53. Third, the cell cycle analysis revealed increased G_1 and G_2 phase fractions and decreased S-phase compartment in HCT116 $p53^{+/+}$ cells after 24 h treatment with **6e** and **3** but not with **4** (Figure 5d, the first line), although the tested concentration of **4** could induce apoptosis in HCT116 $p53^{+/+}$ cells (Supporting Information, Figure S3). In contrast, neither **6e** nor **3** induced cell cycle arrest in HCT116 $p53^{-/-}$ cells, confirming that **6e** exhibited MDM2 inhibition, as did **3**, in tumor cells because cell cycle arrest mediated by cyclin-dependent kinase inhibitor p21 was the major cellular consequence of MDM2-p53 inhibition[21] (Figure 5d, the second line). It is illustrated that compared to **4**, which only binds Bcl-2, **6e** induced p53-mediated cell cycle arrest in addition to the induction of apoptosis due to its MDM2 targeting, which was revealed subsequently by targeting Bcl-2.

Consequently, the Bcl-2 targeting effect of **6e** was examined in DMS53 cells carrying mutant p53 to avoid interference from p53 activation of the Bcl-2 pathway. **4** was tested as a positive control. **6e** treatment led to a dose-dependent disruption of Bcl-2 and Mcl-1 interactions with Bim and Bax, while **4** selectively disrupted Bcl-2 interactions, consistent with their binding profiles (Figure 5e). Accompanying the disruption of these complexes, hallmarks of MOMP, including caspase-3 cleavage, cytochrome c release, and PARP cleavage, were observed (Figure 5e). Notably, compound **3** was also tested. As shown in Figure 5e, compound **3** could not compete with native BH3 partners complexed with Bcl-2/Mcl-1 in living DMS53 cells, even at the high dose of 10 μM, demonstrating that compound **3** is not a real dual inhibitor targeting both p53 and Bcl-2 pathways. This is consistent with previous reports that molecules with affinities to Bcl-2 protein in the 10 μM range cannot disrupt Bcl-2 heterodimers in cells.[30]

These results demonstrated a dual target-based antitumor function of **6e**: (1) **6e** binds to MDM2, releasing p53 from the p53/MDM2 complex and triggering cell cycle arrest via the transcriptional activity of p53, and (2) at the mitochondrial level, **6e** directly binds to antiapoptotic Bcl-2 and Mcl-1, liberating pro-apoptotic proteins from complexes and eventually inducing Bax/Bak-dependent apoptosis.

CONCLUSION

In the present study, we have designed, synthesized, and evaluated a series of new Bcl-2/MDM2 dual inhibitors. On the basis of a pyramid-like *ortho*-triarenes scaffold with a rotatable C−N bond, we obtained a universal inhibitor, **6e**, which could adjust itself to adopt to different α-helixes with different helicities of MDM2 and Bcl-2 and that balances the different bulks of their hotspot residues. **6e** exhibited balanced submicromolar direct binding affinities with MDM2, Bcl-2, and Mcl-1 proteins and potent competition with their native partners, both in vitro and in living tumor cells. It then exhibited cell cycle arrest in addition to the induction of apoptosis due to its p53/Bcl-2 dual targeting ability. To our knowledge, this is the first universal inhibitor that exhibits concomitant inhibition of Bcl-2 and MDM2 in living cells.

MATERIALS AND METHODS

Chemistry. All commercial reagents were purchased and used without further purification unless otherwise stated. ^{1}H NMR spectra were obtained with a Bruker AV-400 spectrometer with chemical shifts reported as ppm (in DMSO, TMS as an internal standard). High-resolution mass spectra (HRMS) were obtained on a HPLC-Q-Tof MS (Micro) spectrometer. Column chromatography was performed on silica gel 200−300 mesh. The purity of all final products was determined by analytical HPLC to be ≥95%. HPLC purity of compounds was measured with a normal-phase HPLC (XBridge C18, 4.6 mm × 150 mm, 5 μm) with two diverse wavelength detection systems. Compounds were eluted by gradient elution of 40/60 to 0/100 H_2O/CH_3OH over 30 min at a flow rate of 0.3 mL/min.

Cell Lines. Cell lines HCT116 $p53^{+/+}$, HCT116 $p53^{-/-}$, and DMS53 were purchased from the Cell Bank of Chinese Academy of Sciences and used within 6 months from resuscitation. Cells were cultured in RPMI 1640 media (Thermo Scientific HyClone, Beijing, China) supplemented with 10% fetal bovine serum (FBS; Gibco BRL, Grand Island, NY, USA) and 100 U/mL penicillin and streptomycin at 37 °C and 5% CO_2.

Reagents, Peptides, and Antibodies. The compounds **3**, **4**, (−)-gossypol, and etoposide were obtained from Selleck Chemicals (Houston, TX, USA). A 21-residue Bid BH3 peptide (residues 79−99) bearing a 6-carboxyfluorescein succinimidyl ester fluorescence tag (FAM-Bid) and a 15-residue p53 TAD peptide (residue 14−29) bearing a 6-carboxyfluorescein succinimidyl ester fluorescence tag (FAM-p53) were synthesized at HD Biosciences (Shanghai, China). The primary antibodies against MDM2, p21, Bax, caspase-3, PARP, and actin were purchased from Santa Cruz Biotechnology (Santa Cruz, CA, USA). The antibodies against p53, phospho-p53 (ser15), Bim, cytochrome c, Bcl-2, and Mcl-1 were purchased from Cell Signaling Technology (New England Biolabs Ltd. Hitchin, UK).

DOI: 10.1021/acs.jmedchem.5b01913
J. Med. Chem. 2016, 59, 3152−3162

Protein Expression and Purification. The plasmid expressing Mcl-1 was constructed as described in our previous study.[31] The plasmid expressing Bcl-2 protein was provided by Renxiao Wang (Shanghai Institute of Organic Chemistry, Chinese Academy of Sciences). The N-terminal domain of human MDM2 (residues 25−108) was cloned into the pET28a (+) vector. The three proteins with an *N*-terminal 8 × His tag were produced in *Escherichia coli* BL21 (DE3) cells. Cells were grown at 37 °C in LB containing 30 μg/mL Kana. Protein expression was induced by 0.4 mM IPTG at 37 °C for 4 h. Cells were lysed in PBS containing 1 μg/mL leupeptin/aprotinin. The protein was purified from the soluble fraction using Ni-NTA resin (Qiagen, Hilden, Germany), following the manufacturer's instructions. The protein was further purified on a Source Q15 column in 25 mM Tris pH 8.0 buffer, with a NaCl gradient. For NMR samples, cells were grown in M9 media supplemented with ^{15}N ammonium chloride.

FP. For the competitive binding assay for the Mcl-1 and Bcl-2 protein, FAM-Bid peptide (10 nM), Mcl-1 protein (55 nM), and Bcl-2 protein (140 nM) were preincubated in the assay buffer (100 mM potassium phosphate, pH 7.5; 100 μg/mL bovine gamma globulin; 0.02% sodium azide). Next, serial dilutions of compounds were added. After a 30 min incubation, the polarization values were measured using the Spectra Max M5 Detection System in a black 96-well plate. Saturation experiments determined that FAM-Bid binds to the Mcl-1 and Bcl-2 proteins with K_d values of 1.9 and 8 nM, respectively. The K_i value for each inhibitor was calculated using the equation we have developed for FP-based assays.[32]

For the competitive binding assay for the MDM2 protein, FAM-p53TAD peptide (20 nM), and MDM2 protein (720 nM) were preincubated in the assay buffer (100 mM potassium phosphate, pH 7.5; 100 μg/mL bovine gamma globulin; 0.02% sodium azide). Next, serial dilutions of compounds were added. After a 30 min incubation, the polarization values were measured using the Spectra Max M5 detection system in a black 96-well plate. Saturation experiments determined that FAM-p53TAD binds to the MDM2 protein with a K_d value of 233 nM, respectively. The K_i value for each inhibitor was calculated using the equation we have developed for FP-based assays.

ITC. The protein−ligand interactions were characterized using an isothermal titration microcalorimeter, ITC200 (GE Healthcare/MicroCal), at 25 °C. A typical experiment included the injection of 19 aliquots (2.1 μL each) containing approximately 0.2 mM ligand solution into a protein solution of approximately 10−20 μM in the ITC cell (in a total volume of approximately 200 μL). An additional set of injections was run in a separate experiment with buffer instead of the protein solution as a control. Before data analysis, the control values were subtracted from the main experimental data.[21]

The binding isotherms were integrated to give the enthalpy change (ΔH), plotted as a function of the molar ratio of the ligand. When necessary, prior to the integration procedures, the baseline was manually adjusted to minimize the background noise. The initial titration point was always discarded. The ΔH/molar ratio plot was a sigmoidal, representing the fractional saturation of the binding sites by the ligand. The Origin 7.0-based software provided by GE/MicroCal was used for data analysis, and the one set of sites model was used as the basic option. The association constant K_a ($1/K_d$) was determined from the slope of the central linear part of the fractional saturation curve. The Gibbs free energy change (ΔG) and entropy change (ΔS) were calculated based on the following equations: $\Delta G = -RT \ln K_a = \Delta H - T\Delta S$, where ΔH was derived from the original ΔH/molar ratio plots.

Molecular Docking. The 3D structures of the human Mcl-1 (hMcl-1; PDB 2NLA) and MDM2 (MDM2; PDB 1YCR) were obtained from the RCSB Protein Data Bank. The 3D structures of the inhibitors were generated using Chembio3D Ultra 11.0 followed by energy minimization. The AutoDock 4.0 program equipped with ADT was used to perform the automated molecular docking. Grid maps covering residues that were perturbed by more than the threshold value of 0.1 ppm in the BH3 binding groove of the Mcl-1 protein and the p53 binding groove of the MDM2 protein were defined for all inhibitors in the AutoDock calculations using a grid spacing of 0.375 Å. The GA-LS algorithm was adopted using default settings. For each docking job, 100 hybrid GA-LS runs were carried out. A total of 100 possible binding conformations were generated and grouped into clusters based on a 1.0 Å cluster tolerance. The docking models were analyzed and represented using ADT.

^{1}H−^{15}N HSQC. Human Mcl-1 (172−321 amino acids) and MDM2 (1−118 amino acids) was prepared as described previously. For NMR studies, BL21 was grown in M9 media supplemented with ^{15}N ammonium chloride to produce uniformly ^{15}N-labeled proteins. Soluble Mcl-1 and MDM2 protein was purified by Ni^{2+} affinity chromatography. The Mcl-1 NMR samples contained 0.1 mM protein in 80% H_2O/10% DMSO-d_6/10% D_2O, 20 mM sodium phosphate (pH 6.8), 5 mM EDTA, and 3 mM DSS. NMR spectra were recorded on Bruker Avance 600 MHz spectrometer equipped with cryoprobe. ^{1}H−^{15}N HSQC spectra were recorded at 1:1 drug to protein ratios and at a temperature of 35 °C for Mcl-1.[28] The MDM2 NMR samples contained 0.10 mM protein in 80% H_2O/10% DMSO-d_6/10% D_2O, 60 mM deuterated sodium acetate, 60 mM sodium phosphate (pH 7.3), and 3 mM DSS. NMR spectra were recorded on Bruker Avance 600 MHz spectrometer equipped with cryoprobe. ^{1}H−^{15}N HSQC spectra were recorded at 1:1 drug to protein ratios and at a temperature of 15 °C for MDM2.[33] Values of the amide chemical shift changes were calculated as $[(\Delta^1\text{H shift})^2 + (\Delta^{15}\text{N shift} \times 0.2)^2]^{1/2}$ in ppm.

Immunoblotting. Cells were lysed in NP-40 lysis buffer (0.2% NP-40, 142.5 mM KCL, 5 mM $MgCl_2$, 1 mM EGTA, and 20 mM HEPES at pH 7.5) containing 1 mM PMSF, 1 μg/mL aprotinin, 1 μg/mL leupeptin, and 1 μg/mL pepstatin. Protein concentrations were determined by Bradford protein assay (Bio-Rad, Philadelphia, PA, USA). Equal protein concentrations of each sample were subjected to sodium dodecyl sulfate polyacrylamide gel electrophoresis (SDS-PAGE) and electrophoretically transferred to polyvinylidene difluoride membranes. Membranes were blocked with TBS containing 5% skim milk and 0.1% Tween 20 and then probed with specific antibodies. Blots were developed using enhanced chemiluminescence kit (Amersham Biosciences, San Diego, CA, USA) according to the manufacturer's instructions.

Immunoprecipitations. Whole-cell lysates were prepared in Triton X-100 buffer (50 mmol/L Tris-HCl, 150 mmol/L NaCl, 5 mmol/L $MgCl_2$, 1 mmol/L EGTA, 10% glycerol, 1% Triton X-100). Total protein (400 μg) was precleared with 12 μL (of a 50% slurry) of protein A/G beads (Santa Cruz Biotechnology). The cleared lysates were incubated overnight at 4 °C with protein A/G beads pre-exposed for 1 h to anti-Bcl-2 or anti-Mcl-1 antibody. Immunoprecipitates were then washed three times with Triton X-100 buffer and boiled in loading buffer (Invitrogen, Carlsbad, CA, USA). Immunoblotting was performed as described above.

Apoptosis Assays. Phosphatidylserine (PS) exposure was quantified by surface Annexin V-FITC staining. Cells were seeded in each well of 6-well tissue culture plates (5×10^4 cells/well) and, 24 h later, were treated with compounds for 48 h. Control cells were treated with an equivalent concentration of the solvent DMSO. Cells were washed twice with PBS and incubated with a 1:40 solution of FITC-conjugated Annexin V for 10 min at room temperature. Stained cells were analyzed by flow cytometry.

Quantitative PCR. Cells were seeded in 96-well plates (10^4 cells/well) and 24 h later were treated with compounds for 12 h. Total RNA was extracted using the Trizol reagent method (Invitrogen) and purified with RNAeasy columns (Qiagen). Aliquots containing 5 μg of total RNA were converted to cDNA using the TaqMan RT reagents kit (Applied Biosystems). The relative quantities of the p53 and p21 transcripts were determined by TaqMan using gene-specific primer/probe sets and 18S RNA as a normalization control. The sequence of the primers and probes was as follows: p53 (F, CTGGGACGGAACAGCTTTGA; R, CCTTTCTTGCGGAGATTCTCTTC; probe, CTGTGCGCCGGTCTCTCCCAGTA), P21 (F, CTGAGACTCTCAGGGTCGAA; R, CGGCGTTTGGAGTGGTAGAA; probe, TTGGCTCACTGCAAGCTCGCCCTT).

Analysis of Cell Cycle Progression. Cells were seeded in a 25 cm^2 flask (10^6 cells/flask) and, 24 h later, were treated with compounds for 24 h. Cells were trypsinized, harvested, and fixed in

DOI: 10.1021/acs.jmedchem.5b01913
J. Med. Chem. 2016, 59, 3152−3162

1 mL of 80% cold ethanol in test tubes and incubated at 4 °C for 15 min. After incubation, cells were centrifuged at 1500 rpm for 5 min and cell pellets were resuspended in 500 μL of propidium iodine (10 μg/mL) containing 300 μg/mL RNase (Sigma, MO, USA). Then cells were incubated on ice for 30 min and filtered with nylon mesh. Cell cycle distribution was calculated from 10000 cells with ModFit LT software (Becton Dickinson, CA, USA) using a FACSCalibur instrument (Becton Dickinson, CA, USA).

■ ASSOCIATED CONTENT

Supporting Information

The Supporting Information is available free of charge on the ACS Publications website at DOI: 10.1021/acs.jmedchem.5b01913.

Additional text, table, and three figures with experimental procedures and full NMR, spectroscopic data for all new compounds (PDF)

Molecular formula strings (CSV)

■ AUTHOR INFORMATION

Corresponding Author

*Phone: +86 411 84986032. Fax: +86 411 84986032. E-mail: zczhang@dlut.edu.cn.

Author Contributions

Z.W. and T.S. contributed equally to this work.

Notes

The authors declare no competing financial interest.

■ ACKNOWLEDGMENTS

We thank Prof. Baomin Wang (Dalian University of Technology) for insightful discussion of synthesis. The work was supported by the National Natural Science Foundation of China (21372036, 81570129, 81430083, 21502015, and 21402022).

■ REFERENCES

(1) Azzarito, V.; Long, K.; Murphy, N. S.; Wilson, A. J. Inhibition of alpha-helix-mediated protein-protein interactions using designed molecules. *Nat. Chem.* **2013**, *5*, 161−173.

(2) Becerril, J.; Hamilton, A. D. Helix mimetics as inhibitors of the interaction of the estrogen receptor with coactivator peptides. *Angew. Chem., Int. Ed.* **2007**, *46*, 4471−4473.

(3) Barnard, A.; Long, K.; Martin, H. L.; Miles, J. A.; Edwards, T. A.; Tomlinson, D. C.; Macdonald, A.; Wilson, A. J. Selective and potent proteomimetic inhibitors of intracellular protein-protein interactions. *Angew. Chem., Int. Ed.* **2015**, *54*, 2960−2965.

(4) Lee, J. H.; Zhang, Q.; Jo, S.; Chai, S. C.; Oh, M.; Im, W.; Lu, H.; Lim, H. S. Novel pyrrolopyrimidine-based alpha-helix mimetics: cell-permeable inhibitors of protein-protein interactions. *J. Am. Chem. Soc.* **2011**, *133*, 676−679.

(5) Plante, J. P.; Burnley, T.; Malkova, B.; Webb, M. E.; Warriner, S. L.; Edwards, T. A.; Wilson, A. J. Oligobenzamide proteomimetic inhibitors of the p53-hDM2 protein-protein interaction. *Chem. Commun.* **2009**, *34*, 5091−5093.

(6) Wade, M.; Li, Y. C.; Wahl, G. M. MDM2, MDMX and p53 in oncogenesis and cancer therapy. *Nat. Rev. Cancer* **2013**, *13*, 83−96.

(7) Stiewe, T. The p53 family in differentiation and tumorigenesis. *Nat. Rev. Cancer* **2007**, *7*, 165−168.

(8) Adams, J. M.; Cory, S. The Bcl-2 apoptotic switch in cancer development and therapy. *Oncogene* **2007**, *26*, 1324−1337.

(9) Wade, M.; Rodewald, L. W.; Espinosa, J. M.; Wahl, G. M. BH3 activation blocks Hdmx suppression of apoptosis and cooperates with Nutlin to induce cell death. *Cell Cycle* **2008**, *7*, 1973−1982.

(10) Lee, D. H.; Ha, J. H.; Kim, Y.; Jang, M.; Park, S. J.; Yoon, H. S.; Kim, E. H.; Bae, K. H.; Park, B. C.; Park, S. G.; Yi, G. S.; Chi, S. W. A conserved mechanism for binding of p53 DNA-binding domain and anti-apoptotic Bcl-2 family proteins. *Mol. Cells* **2014**, *37*, 264−269.

(11) Yao, H.; Mi, S.; Gong, W.; Lin, J.; Xu, N.; Perrett, S.; Xia, B.; Wang, J.; Feng, Y. Anti-apoptosis proteins Mcl-1 and Bcl-xL have different p53-binding profiles. *Biochemistry* **2013**, *52*, 6324−6334.

(12) Xu, H.; Ye, H.; Osman, N. E.; Sadler, K.; Won, E. Y.; Chi, S. W.; Yoon, H. S. The MDM2-binding region in the transactivation domain of p53 also acts as a Bcl-X_L-binding motif. *Biochemistry* **2009**, *48*, 12159−12168.

(13) Shin, J. S.; Ha, J. H.; Chi, S. W. Targeting of p53 peptide analogues to anti-apoptotic Bcl-2 family proteins as revealed by NMR spectroscopy. *Biochem. Biophys. Res. Commun.* **2014**, *443*, 882−887.

(14) Ha, J. H.; Won, E. Y.; Shin, J. S.; Jang, M.; Ryu, K. S.; Bae, K. H.; Park, S. G.; Park, B. C.; Yoon, H. S.; Chi, S. W. Molecular mimicry-based repositioning of nutlin-3 to anti-apoptotic Bcl-2 family proteins. *J. Am. Chem. Soc.* **2011**, *133*, 1244−1247.

(15) Yin, H.; Lee, G. I.; Park, H. S.; Payne, G. A.; Rodriguez, J. M.; Sebti, S. M.; Hamilton, A. D. Terphenyl-based helical mimetics that disrupt the p53/HDM2 interaction. *Angew. Chem., Int. Ed.* **2005**, *44*, 2704−2707.

(16) Yin, H.; Lee, G. I.; Sedey, K. A.; Kutzki, O.; Park, H. S.; Orner, B. P.; Ernst, J. T.; Wang, H. G.; Sebti, S. M.; Hamilton, A. D. Terphenyl-based bak BH3 alpha-helical proteomimetics as low-molecular-weight antagonists of Bcl-X_L. *J. Am. Chem. Soc.* **2005**, *127*, 10191−10196.

(17) Li, X.; Wang, Z.; Feng, Y.; Song, T.; Su, P.; Chen, C.; Chai, G.; Yang, Y.; Zhang, Z. Two-face, two-turn alpha-helix mimetics based on a cross-acridine scaffold: analogues of the Bim BH3 domain. *ChemBioChem* **2014**, *15*, 1280−1285.

(18) Guichard, G.; Huc, I. Synthetic foldamers. *Chem. Commun.* **2011**, *47*, 5933−5941.

(19) Mathew, S. M.; Engle, J. T.; Ziegler, C. J.; Hartley, C. S. The role of arene-arene interactions in the folding of *ortho*-phenylenes. *J. Am. Chem. Soc.* **2013**, *135*, 6714−6722.

(20) He, J.; Crase, J. L.; Wadumethrige, S. H.; Thakur, K.; Dai, L.; Zou, S.; Rathore, R.; Hartley, C. S. *ortho*-Phenylenes: unusual conjugated oligomers with a surprisingly long effective conjugation length. *J. Am. Chem. Soc.* **2010**, *132*, 13848−13857.

(21) Vassilev, L. T.; Vu, B. T.; Graves, B.; Carvajal, D.; Podlaski, F.; Filipovic, Z.; Kong, N.; Kammlott, U.; Lukacs, C.; Klein, C.; Fotouhi, N.; Liu, E. A. In vivo activation of the p53 pathway by small-molecule antagonists of MDM2. *Science* **2004**, *303*, 844−848.

(22) Shin, J. S.; Ha, J. H.; He, F.; Muto, Y.; Ryu, K. S.; Yoon, H. S.; Kang, S.; Park, S. G.; Park, B. C.; Choi, S. U.; Chi, S. W. Structural insights into the dual-targeting mechanism of Nutlin-3. *Biochem. Biophys. Res. Commun.* **2012**, *420*, 48−53.

(23) Oltersdorf, T.; Elmore, S. W.; Shoemaker, A. R.; Armstrong, R. C.; Augeri, D. J.; Belli, B. A.; Bruncko, M.; Deckwerth, T. L.; Dinges, J.; Hajduk, P. J.; Joseph, M. K.; Kitada, S.; Korsmeyer, S. J.; Kunzer, A. R.; Letai, A.; Li, C.; Mitten, M. J.; Nettesheim, D. G.; Ng, S.; Nimmer, P. M.; O'Connor, J. M.; Oleksijew, A.; Petros, A. M.; Reed, J. C.; Shen, W.; Tahir, S. K.; Thompson, C. B.; Tomaselli, K. J.; Wang, B.; Wendt, M. D.; Zhang, H.; Fesik, S. W.; Rosenberg, S. H. An inhibitor of Bcl-2 family proteins induces regression of solid tumours. *Nature* **2005**, *435*, 677−681.

(24) Kussie, P. H.; Gorina, S.; Marechal, V.; Elenbaas, B.; Moreau, J.; Levine, A. J.; Pavletich, N. P. Structure of the MDM2 oncoprotein bound to the p53 tumor suppressor transactivation domain. *Science* **1996**, *274*, 948−953.

(25) Fire, E.; Gulla, S. V.; Grant, R. A.; Keating, A. E. Mcl-1-Bim complexes accommodate surprising point mutations via minor structural changes. *Protein Sci.* **2010**, *19*, 507−519.

(26) Liu, X. Q.; Dai, S. D.; Zhu, Y. N.; Marrack, P.; Kappler, J. W. The structure of a Bcl-xL/Bim fragment complex: implications for bim function. *Immunity* **2003**, *19*, 341−352.

(27) Dutta, S.; Gulla, S.; Chen, T. S.; Fire, E.; Grant, R. A.; Keating, A. E. Determinants of BH3 binding specificity for Mcl-1 versus Bcl-xL. *J. Mol. Biol.* **2010**, *398*, 747−762.

DOI: 10.1021/acs.jmedchem.5b01913
J. Med. Chem. 2016, 59, 3152−3162

(28) Jiang, J.-A.; Huang, W.-B.; Zhai, J.-J.; Liu, H.-W.; Cai, Q.; Xu, L.-X.; Wang, W.; Ji, Y.-F. 'One-pot' synthesis of 4-substituted 1,5-diaryl-1H-pyrazole-3-carboxylates via lithium tert-butoxide-mediated sterically hindered Claisen condensation and Knorr reaction. *Tetrahedron* **2013**, *69*, 627−635.
(29) Carpino, P. A.; Griffith, D. A.; Sakya, S.; Dow, R. L.; Black, S. C.; Hadcock, J. R.; Iredale, P. A.; Scott, D. O.; Fichtner, M. W.; Rose, C. R.; Day, R.; Dibrino, J.; Butler, M.; Debartolo, D. B.; Dutcher, D.; Gautreau, D.; Lizano, J. S.; O'Connor, R. E.; Sands, M. A.; Kelly-Sullivan, D.; Ward, K. M. New bicyclic cannabinoid receptor-1 (CB1-R) antagonists. *Bioorg. Med. Chem. Lett.* **2006**, *16*, 731−736.
(30) Zhang, Z.; Li, X.; Song, T.; Zhao, Y.; Feng, Y. An anthraquinone scaffold for putative, two-face Bim BH3 alpha-helix mimic. *J. Med. Chem.* **2012**, *55*, 10735−10741.
(31) Liu, Q.; Wang, H. G. Anti-cancer drug discovery and development: Bcl-2 family small molecule inhibitors. *Commun. Integr. Biol.* **2012**, *5*, 557−565.
(32) Zhang, Z.; Song, T.; Zhang, T.; Gao, J.; Wu, G.; An, L.; Du, G. A novel BH3 mimetic S1 potently induces Bax/Bak-dependent apoptosis by targeting both Bcl-2 and Mcl-1. *Int. J. Cancer* **2011**, *128*, 1724−1735.
(33) Uhrinova, S.; Uhrin, D.; Powers, H.; Watt, K.; Zheleva, D.; Fischer, P.; McInnes, C.; Barlow, P. N. Structure of free MDM2 N-terminal domain reveals conformational adjustments that accompany p53-binding. *J. Mol. Biol.* **2005**, *350*, 587−598.

DOI: 10.1021/acs.jmedchem.5b01913
J. Med. Chem. 2016, 59, 3152−3162